Journal of Luminescence 246 (2022) 118856

Contents lists available at ScienceDirect

Journal of Luminescence

journal homepage: www.elsevier.com/locate/jlumin

Deep blue photoluminescence and optical gain from sodium-doped carbon dots

Zhenxu Lin [a], Jiaxin Yang [a], Qiwen Zeng [b], Shaolong Tie [b,**], Rui Huang [c,***], Sheng Lan [a,*]

[a] Guangdong Provincial Key Laboratory of Nanophotonic Functional Materials and Devices, School of Information and Optoelectronic Science and Engineering, South China Normal University, Guangzhou, 510006, China
[b] School of Chemistry, South China Normal University, Guangzhou, 510006, China
[c] School of Material Science and Engineering, Hanshan Normal University, Chaozhou, 521041, China

ARTICLE INFO

Keywords:
Sodium-doped carbon dots
Deep blue photoluminescence
Optical gain
Amplified spontaneous emission

ABSTRACT

The photoluminescence (PL) from carbon dots can be dramatically modified through the engineering of surface oxygen-containing functional groups. Despite the recent surge of interest in the non-metal doping of carbon dots, the photo-physical properties of metal-doped carbon dots remain unexplored. Here, we report the highly efficient deep blue PL and amplified spontaneous emission from sodium (Na)-ion-doped carbon dots. Based on the structure- and temperature-dependent PL and the temporal evolution of PL, we reveal that the introduction of Na ions into carbon dots not only passivate the electronegative oxygen related defects but also create new Na–O related defect centers in the band gap, leading to deep blue PL with dramatically reduced bandwidth and significantly enhanced quantum yield. We establish a luminescence model with four energy levels to interpret the PL dynamics of Na^+-doped carbon dots. We demonstrate for the first time the ASE from such carbon dots, which exhibit a net optical gain coefficient of 47.8 cm^{-1} at 440 nm. Our results open new horizons for improving the PL of carbon dots and pave the way for realizing optoelectronic devices based on carbon dots.

1. Introduction

Carbon materials, which possess richness of electronic and optical properties such as high mobility, high surface area and high photoluminescence quantum yields (PL QYs), has currently attracted intensive attention due to their promising applications in energy storage, bioluminescence imaging and optoelectronic device [1–5]. Sodium (Na) ion batteries with carbon based anodes have been emerging as one of the most promising building blocks in the next generation green electrochemical energy storage devices because of their abundant constituent elements and low-cost compared with lithium (Li) [5–8]. Unfortunately, the low capacities of ~35 mA h/g prevent their further practical applications. The main issue hindering the high capacities of Na ion batteries with carbon based anodes stem from the larger ionic radii of Na^+ which blocking the intercalation of Na^+ in carbon materials. Consequently, more attention has been focused on the intercalation behavior of Na^+ into carbon materials and the Na^+ storage mechanism of hard carbon in order to improve their electrochemical performance [8–11]. So far, due to the few-layer carbon structure which can promote the intercalation and mobility of Na^+, low-dimensional carbon materials, such as graphene sheets, carbon dots (C-dots), and carbon nanotubes, is considered to be excellent electrode materials for Na ion batteries [4–6]. For example, the Na ion batteries with Janus graphene stacks anode show a capacity of ≈332 mA h/g which can compared with the Li ion batteries [5]. In addition, defects such as functional group and vacancy in carbon structure also can promote the formation of sodiophilic interphase and enhance the storage of Na^+ for high-performance Na ion batteries. The defective graphene based electrode theoretically can achieve a high specific capacity of ~1117 mA h/g for Na ion batteries [9]. However, except the advance of the enhanced electrochemical storage properties from Na^+ doped carbon materials, few studies have focused on the photophysical characterizations of Na^+ doped C-dots, especially their further optoelectronic applications. In particular, because the PL characteristics of C-dots is mainly affected by the surface configuration, the analysis of the photophysical properties of Na^+ doped C-dots would contribute to understand the intercalation behavior of Na^+

* Corresponding author.
** Corresponding author.
*** Corresponding author.
E-mail addresses: tiesl@scnu.edu.cn (S. Tie), rhuang@hstc.edu.cn (R. Huang), slan@scnu.edu.cn (S. Lan).

https://doi.org/10.1016/j.jlumin.2022.118856
Received 30 November 2021; Received in revised form 3 March 2022; Accepted 24 March 2022
Available online 25 March 2022

doping in the carbon materials.

Recently, compared with heavy metal ions quantum dots (QDs) such as Cd^{2+} and Pb^{2+} based QDs, which generally feature narrow bandwidth emission with high QY [12–19], luminescent C-dots have regarded as a promising material for high-definition displays, energy-efficient solid--state light emitting devices (LEDs) and low threshold lasers because of their superior optical properties and environmental friendliness [20–22]. Luminescent C-dots with tunable color and high QY have been successfully achieved via the oxidation and/or reduction of surface oxygen functional groups [23–29]. For example, a surface amination method was employed to eliminate the oxygen-containing functional groups in C-dots, leading to high-performance deep blue LEDs with an EQE of 4% [28]. In addition, metal doping is also considered as an effective way to obtain highly-efficient luminescent C-dots because of the donor nature of metal ions [30–34]. Up to now, a variety of metal ions, such as Zn^{2+}, Mn^{2+}, K^{+}, and Cu^{2+}, have been used to enhance the PL of C-dots [33–36]. In fact, an effective blue light emission from C-dots has been achieved though the Na^{+} modification of functional group [33]. However, the physical mechanism of Na^{+} doping for the enhanced PL of C-dots and the dynamics of carrier recombination in Na^{+} doped C-dots remain unclear. In particular, the Na^{+} doped C-dots emitting deep blue light with narrow linewidth (full width at half maxima or FWHM) have not yet been achieved. Moreover, the amplified spontaneous emission (ASE) from Na^{+} doped C-dots has never been reported.

In this work, we report the synthesis and optical characterization of sodium (Na)-ion-doped C-dots that emit highly efficient deep blue PL with narrow linewidth. We reveal that reduced PL linewidth and the enhanced PL QY observed for Na^{+}-doped C-dots originate from the elimination of oxygen-containing functional groups on the surfaces of C-dots. Based on the temporal evolution of the PL spectrum, it is found that the incorporation of Na^{+} into C-dots creates new Na–O coordinating functional knots in the middle of the bandgap, which act as defect luminescent centers and contribute dominantly to the deep blue PL of C-dots. Moreover, we successfully interpret the PL dynamics of Na^{+}-doped C-dots with a four-level luminescence model and demonstrate for the first time the ASE in a polymer film doped with such C-dots.

2. Materials & methods

2.1. Preparation of Na^{+}-doped C-dots and thin films

Na^{+}-doped C-dots studied in this work were prepared via a modified solid-state reaction with the different C/Na molar ratio. Firstly, an ethanol solution was obtained by dissolving 0.1 M (0.4 g) sodium hydroxide with 5 mL ethanol. Then, 0.1 M (2.10 g) citric acid monohydrate and 0.1 M (2.94 g) trisodium citrate dehydrate were put into two mortars independently for grinding in ethanol. Meanwhile, the above sodium hydroxide ethanol solution was dropped into the mortars to form the mixed C–Na precursor with the C/Na molar ratio of 1 : 0.32 and 1 : 1.28, which were named as sample-L and sample-H, respectively. Once thick porridge-like mixtures were obtained, they were transferred to two beakers and dried in a vacuum oven for 2 h at 60 °C and 180 °C, respectively. After cooling to room temperature, samples denoted as L and H were obtained. The crude C-dots product of solid-state reaction was dialyzed using a dialysis bag (1000 Da) for 48 h (replaced deionized water every 24 h) against deionized water to remove the excess impurities and salt. Finally, the Na^{+}-doped C-dots powder was dispersed in ethanol aqueous solution with the concentration of 10 mg/mL. Thin films of Na^{+}-doped C-dots were obtained by drop-casting 50–100 μl of Na^{+}-doped C-dots ethanol aqueous solution at ambient conditions onto quartz substrates, followed by drying in a vacuum drying oven for 24 h at ambient conditions.

2.2. Characterization of Na^{+}-doped C-dots

The microstructure and composition of the Na^{+}-doped C-dots were characterized by using high resolution transmission electron microscopy (HR-TEM) and energy dispersive spectroscopy (EDS), respectively. The bonding configuration of Na^{+}-doped C-dots was examined by using Fourier transform infrared (FTIR) spectra. The absorption spectra were measured by using a spectrophotometer (UV-3600, Shimadzu). The PL measurements, including the temperature dependent PL spectra, the temporal evolution of the PL spectra, and the QY evaluation, were carried out by using a PL spectrometer (FLS1000, Edinburgh Instrument). The characterization of the optical gain for the thin films of Na^{+}-doped C-dots was performed by using the standard variable stripe length (VSL) technique in a Raman microscope (LabRAM HR Evolution) equipped with a 325-nm He–Cd laser.

3. Result and discussion

We first examined the microstructure of Na^{+}-doped C-dots by HR-TEM. A typical example is shown in Fig. 1a and Figure S1 in which the lattice constant of C-dots was found to be ~0.22 nm, in good agreement with the lattice constant of graphite in the <100> direction [37]. In Fig. 1b, we present the EDS spectra measured for the two samples. It can be seen that the contents of Na and O in sample-H (12.01% and 33.17%) are much higher than those in sample L (3.94% and 22.97%). The increase in the contents of Na and O is compensated by the reduction in the content of C, which is reduced from 73.09% to 54.83%. We employed FTIR absorption spectra to detect the local bonding configurations of Na^{+}-doped C-dots, as shown in Fig. 1d. The broad absorption band peaking at 3380 cm^{-1} with a shoulder at 2940 cm^{-1} are attributed to the O–H and C–H stretching vibration, respectively [38]. The two distinct absorption bands at 1405 and 1590 cm^{-1} are ascribed to the C–O and C═O stretching vibrations of sodium carboxyl groups, respectively [39]. In addition, the absorption peaks located at 1070 and 1257 cm^{-1} are related to the stretching vibrations of C–O (alkoxy) and C–O (epoxy) bonds, respectively [40]. The chemical structure of Na^{+}-doped carbon dots is illustrated in Fig. 1e. It is remarkable that the absorptions related to the C–O and C═O stretching vibrations of sodium carboxyl groups are enhanced in sample-H as compared with sample-L. In addition, the two absorption bands become sharper and narrower in sample-H, implying a reduction in structure defect. Moreover, the absorption band of C–O (alkoxy) and C–O (epoxy) bonds disappear completely with the absorption band of O–H bond is dramatically attenuated in sample-H. These changes are expected from the reduction of O in sample-H, which is determined by the EDS analysis.

In Fig. 1c, we compare the emission and excitation spectra measured for the two samples dissolved in ethanol aqueous solution. For sample-L, the PL spectrum exhibits a broad band peaking at 465 nm. The bandwidth (FWHM) is estimated to be ~113 nm. In the PLE spectrum, one can see a broad band peaking at 380 nm and a shoulder at ~330 nm. It can be attributed to the electronic transition from the highest occupied molecular orbital (HOMO) and the lowest unoccupied molecular orbital (LUMO) [41]. It is found that the PL peak exhibits a dependence on the wavelength of the excitation light (see Figure S2). This phenomenon was previously observed in most C-dots and it was attributed to the surface state emission of oxygen-containing functional groups, such as OH and COOH groups [23,40]. In sample-H, the PL peak is blueshifted from 465 to 438 nm. Meanwhile, a dramatic reduction of the bandwidth from ~113 to ~65 nm is observed. The PLE spectrum is also blueshifted to 315 nm with a narrower bandwidth. Moreover, a new weak absorption band located at 315 nm appears in the absorption spectrum (see Figure S3), which can be ascribed to the energy trapping of the surface defect state [41]. More importantly, we observed a PL QY as high as 19.36% in sample-H, which is significantly improved by more than one order of magnitude as compared to the value of sample-L (~1.45%) (see Figure S4). As a result, one can easily observe the strong blue light emission from sample H under day light, which is generated at an excitation wavelength of 325 nm. Interestingly, the PL peak and bandwidth of sample-H are nearly independent of the excitation wavelength

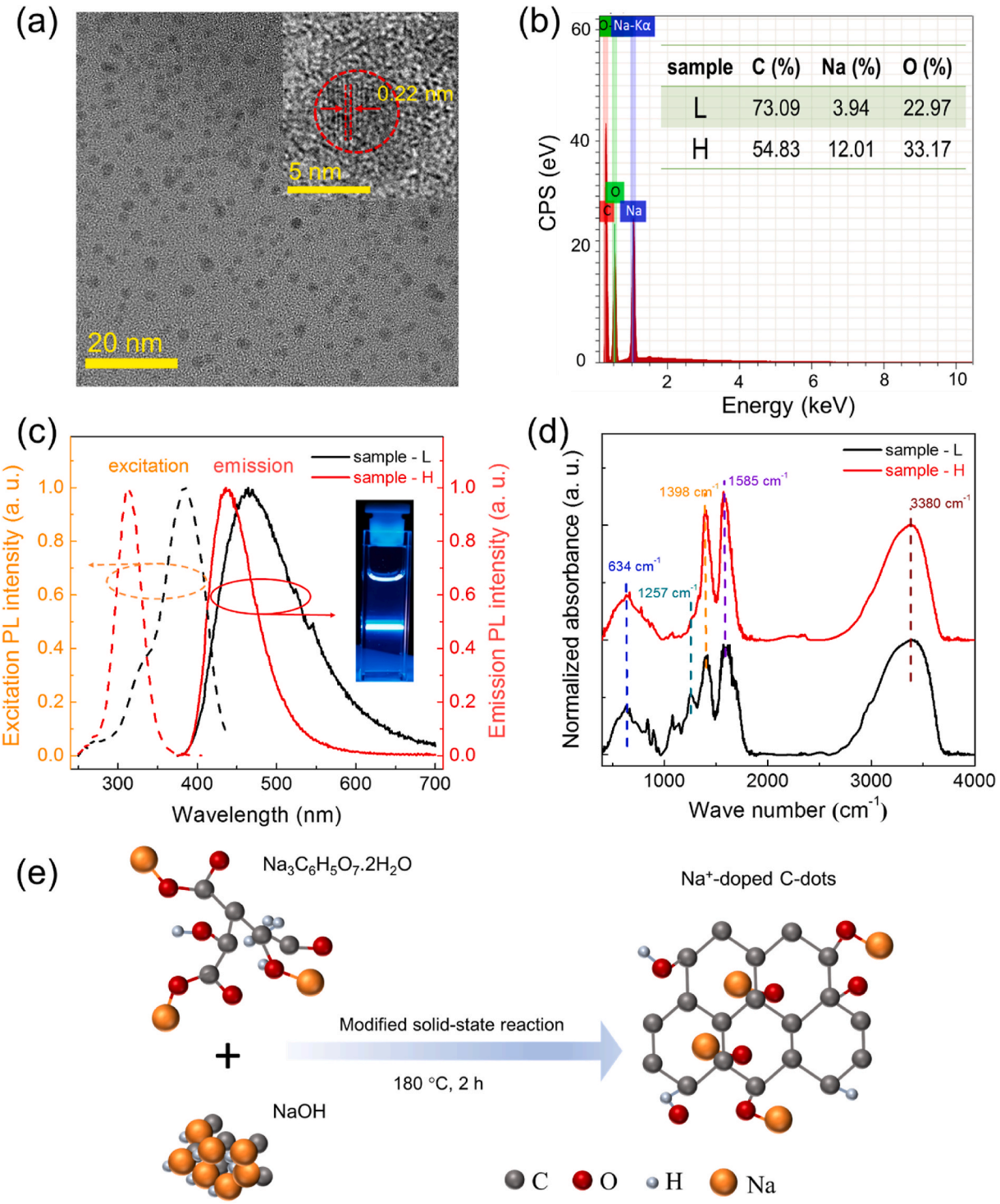

Fig. 1. (a) TEM image of sample-H. A magnified image in which the lattice constant can be extracted is shown in the inset. (b) EDS of sample-H. A comparison of the C, Na and O contents in sample-L and sample-H based on the EDS is shown in the inset. (c) Normalized excitation and emission spectra measured for sample-L and sample-H. The inset shows the emission from sample-H dispersed in the aqueous solution of ethanol under the excitation of 325-nm light. (d) Comparison of the FTIR spectra of sample-L and sample-H. (e) Illustration of formation process and chemical structure of Na^+-doped carbon dots (sample-H).

(see Figure S5). The distinct PL and PLE spectra of sample-L and sample-H indicate completely different physical origins for electronic transition and the crucial roles of Na^+ doping in modifying the luminescence properties and in improving PL QYs.

In order to gain a deep insight into Na^+ doping, we performed the transient PL measurements for the two samples, as shown in Fig. 2a and 2b. Different from the PL spectrum in the stead state, the transient PL spectra of sample-L exhibits a broadband centered at 475 nm with a small shoulder at 435 nm. This behavior implies that two different electronic transitions with emission wavelengths at 435 and 475 nm are involved in the blue emission from the ethanol aqueous solution of Na^+-doped C-dots. With increasing the concentration of Na^+, the emission at 435 takes over the dominant role from the emission at 475 nm, suggesting that Na^+ doping introduces a new luminescence center in C-dots.

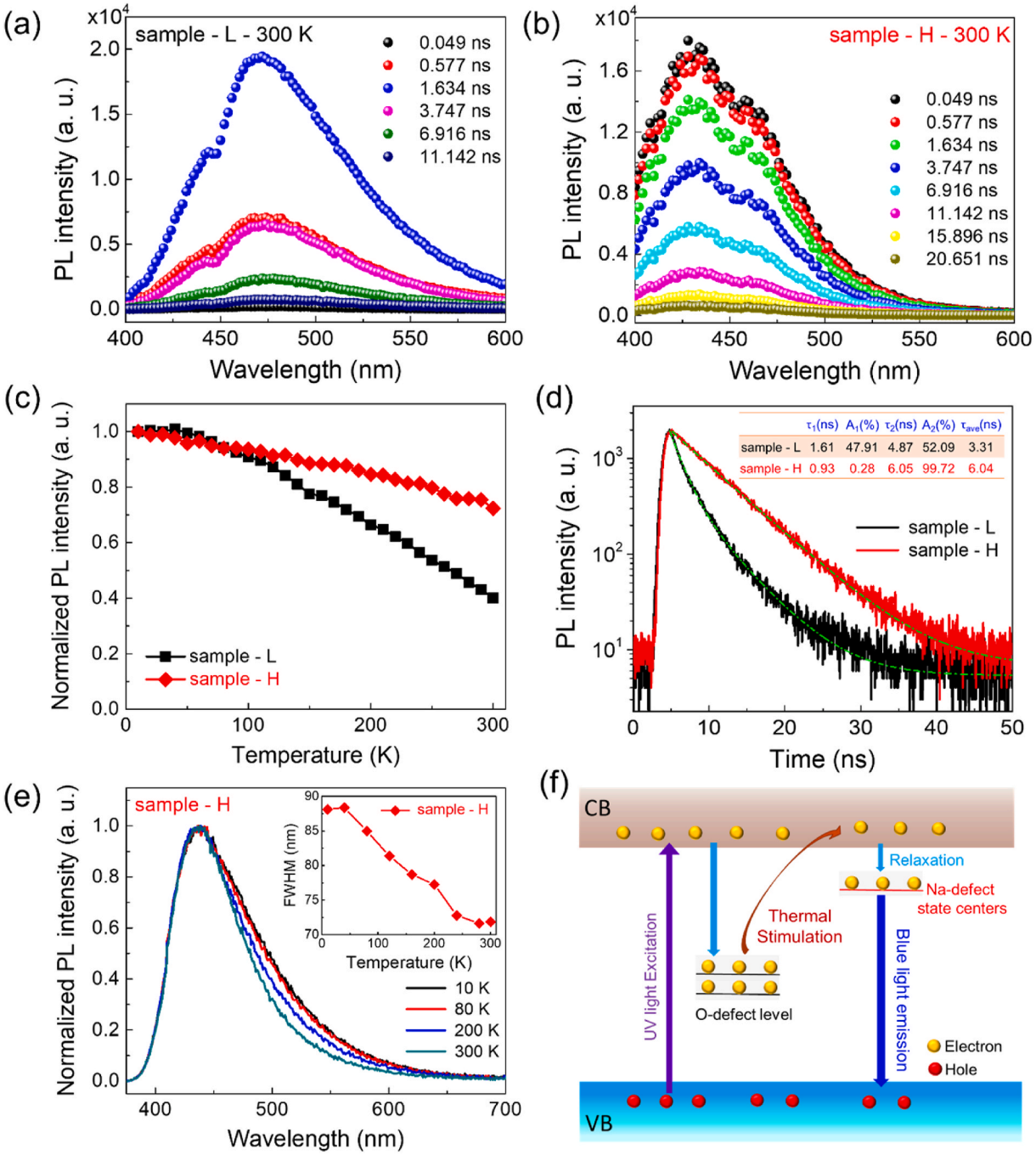

Fig. 2. Transient PL spectra measured for sample-L (a) and sample-H (b) at 300 K. (c) Dependence of the integrated PL intensity on temperature measured for the two samples. (d) PL decays measured for the two samples. They were fitted by using biexponential decay function: $I(t) = I_0+I_1*\exp(-t/\tau_1)+I_2*\exp(-t/\tau_2)$, where I_0 is the background level, I_i and τ_i (i = 1, 2) are the amplitude and lifetime of each exponential decay. The inset shows the fitting results. (e) Normalized PL spectra of sample-H obtained at different temperatures ranging from 10 K to 300 K. The dependence of the PL bandwidth (FWHM) on temperature is shown in the inset. (f) Schematic showing the four-level energy diagram proposed for Na^+-doped C-dots.

It has been known that C-dots doped with metals (such as Zn, and Mn, etc) will create metal-O coordinating functional knots adsorbed on the surfaces, resulting in multi-energy states in C-dots [32,42]. Based on the EDS analysis and the FTIR spectra, it suggests that the oxidation of Na^+ passivates the electronegative oxygen related defects and creates Na–O coordinating functional knots such as sodium carboxyl functional groups, as shown in Fig. 1e. It is considered that Na–O coordinating functional knots may come from O–H, C–O (alkoxy) and C–O (epoxy) bonds because of their acceptor nature. This suspect can be used to interpret the narrowing of the PL band with increasing concentration of Na^+. Therefore, we believe that the PL band centered at 435 nm may originate from the surface luminescent centers related to Na–O coordinating functional knots.

In Fig. 2c, we show the temperature-dependent PL intensity measured for the two samples. In both cases, a reduction of the PL intensity is observed with increasing temperature due to the thermal activation of non-radiative recombination channels. When the temperature is raised from 10 to 300 K, the PL intensity of sample-L drops dramatically to ~40% of the original value. In contrast, the PL intensity of sample-H decreases only to 72% of the initial intensity. This behavior

indicates that Na^+ doping can suppress the activation of the non-radiative decay, which is consistent with the enhanced PL efficiency. The PL decays measured at 300 K for the two samples are fitted by using biexponential function, as shown in Fig. 2d. The average lifetimes are found to be ~3.31 and ~6.04 ns for sample-L and sample-H, respectively. The increase of the PL lifetime with increasing Na^+ concentration also verifies the effective suppression of the non-radiative decay channels caused by Na^+ doping.

In Fig. 2e, we present the normalized PL spectra measured for sample-H at different temperatures ranging from 10 to 300 K. It can be seen that the dominant PL peak position remained unchanged with increasing temperature, verifying that the blue emission originates from the radiative recombination of carriers though the luminescent centers [43]. Interestingly, it is found that the linewidth (FWHM) of the PL band decrease gradually from 88 nm to 72 nm when the temperature is increased from 10 to 300 K due to the attenuation of the long wavelength side of the PL band. This behavior is completely different from undoped C-dots in which thermal broadening of the PL band originating from the electron–phonon interaction is observed [43]. In our case, this anomalous behavior can be explained by the de-trapping process of electrons activated by thermal energy in a four-level luminescence model, as shown in Fig. 2f. Upon light excitation, electrons in the valence band are lifted to the high energy states in the conduction band and then rapidly relaxed to the surface defect states created by Na–O coordinating functional knots or oxygen-containing functional groups. Most electrons will radiatively recombine with holes, generating a strong blue emission at ~435 nm. Meanwhile, some electrons are subsequently captured by the deeper state related to oxygen. We examined the persistent PL decay at 465 nm obtained at different temperatures ranging from 10 to 300 K. The samples were excited by 325-nm light for 2.0 min (see Figure S6). At low temperatures, the electrons captured in the oxygen-related defect state cannot hop back to the high-energy excited state due to the lack of thermal energy. In this case, the electrons can only jump to the ground state and recombine with holes, leading to the light emission at 465 nm. Consequently, the bandwidth of the PL spectrum becomes broader with reducing temperature. At room temperature with sufficient thermal energy, the captured electrons can jump from the deep defect state to the high-energy excited state. As a result, the blue light emission can be observed under excited at different wavelengths ranging from 550 nm to 650 nm, as shown in Figure S7. This phenomenon may be exploited to demonstrate population inversion in this system and to realize light amplification based on C-dots [44].

We investigated the amplified spontaneous emission (ASE) from Na^+-doped C-dots by using the variable stripe length (VSL) method, as illustrated in the inset of Fig. 3. The integrated PL intensities from the thin film doped with Na^+-doped C-dots measured at different pump powers under the excitation of 325-nm light are presented in Fig. 3. Apparently, an exponential increase in the integrated PL intensity of the sample-H is observed with increasing the pump power, which indicates the appearance of ASE in the thin film. In Fig. 4, we show the dependence of the PL intensity at 440 nm on the pumping length. One can see that the ASE spectrum of the film appears as a broad emission band peaking at 440 nm. It is consistent with the physical origin of the PL which originates from the surface defect luminescent centers realized to Na–O coordinating functional knots. It is noticed that the ASE intensity exhibits an exponential increase with increasing the pumping length (<1100 μm). The net optical gain coefficient g can be obtained by fitting with the one-dimensional amplifier equation [45,46]:

$$I_{ASE}(l) = \frac{J_{SP}(\Omega)}{g} \cdot (e^{gl} - l).$$

Here, l is the pumping length and $J_{SP}(\Omega)$ is the spontaneous emission intensity. The net optical gain coefficient derived from fitting is $g = 47.8$ cm^{-1}, which is comparable to or even better than the pure C dots medium [44,45]. Our results provide a practical approach to fabricate the

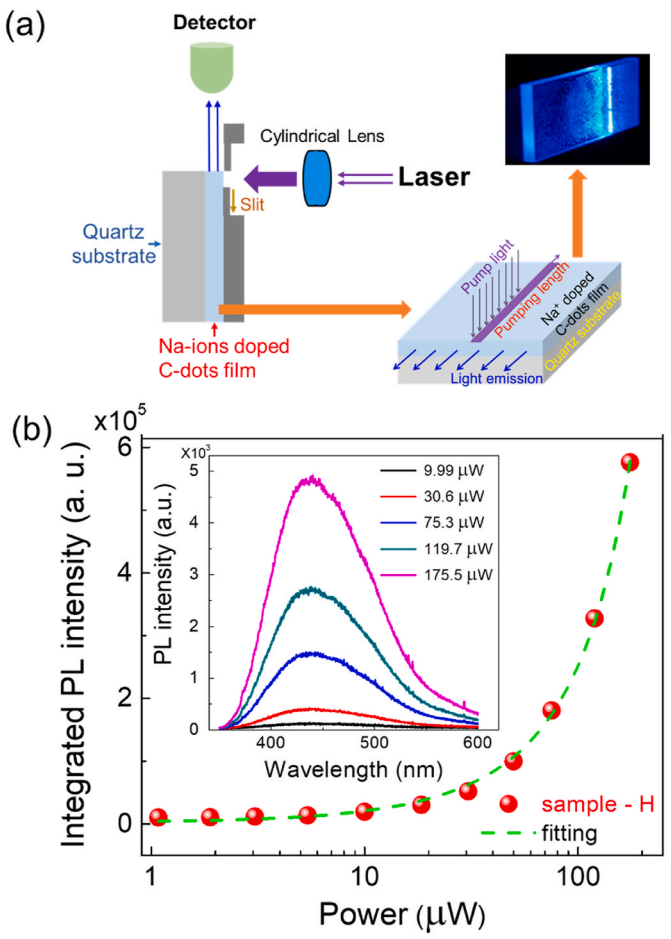

Fig. 3. (a) Schematic showing the VSL method used to investigate the ASE in the film doped with Na^+-doped C-dots. (b) Dependence of the integrated PL intensity from the film on the excitation power. The PL spectra measured at different excitation powers are shown in the inset.

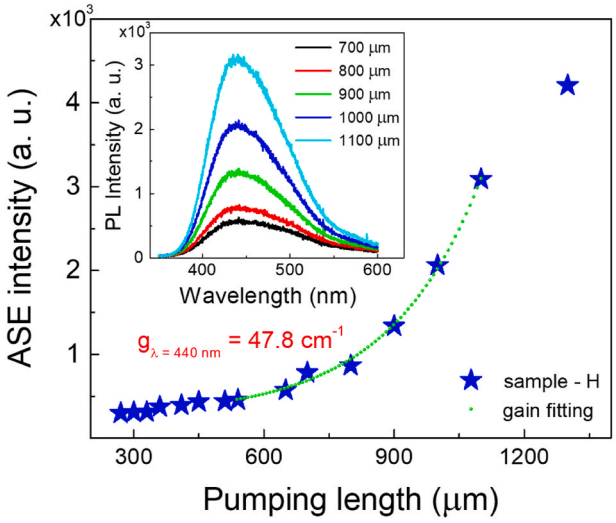

Fig. 4. Dependence of the integrated PL intensity from the film on the pump length. The PL spectra measured at different pumping lengthes shown in the inset.

highly efficient luminescent C-dots for future applications in optoelectronic applications.

4. Conclusions

In summary, we observed highly efficient deep blue PL with narrow bandwidth in Na^+-doped C-dots and demonstrated ASE in a thin film doped with such C-dots. The ethanol aqueous solution of Na^+-doped C-dots exhibited deep blue emission at 438 nm with a narrower linewidth (FWHM) of 65 nm and a QY of ~20%. We revealed that Na^+ doping not only passivates the electronegative oxygen related defects but also introduces Na–O related defect luminescent centers in the band gap, leading to the deep blue emission with reduced bandwidth and enhanced QY. We found a net optical gain coefficient as large as $g = 47.8\ cm^{-1}$ in the film doped with such C-dots and explained the PL and ASE by using a four-level luminescence model. Our findings open new horizons for manipulating the PL of C-dots and pave the way for realizing highly efficient light emitting devices based on Na^+-doped C-dots.

Author statement

Zhenxu Lin : Writing – original draft, Investigation, Formal analysis; **Jiaxin Yang** : Investigation, Formal analysis; **Qiwen Zeng** : Investigation, Formal analysis; **Shaolong Tie** : Conceptualization, Methodology, Validation; **Rui Huang** : Writing- Reviewing and Editing; **Sheng Lan**: Writing- Reviewing and Editing.

Declaration of competing interest

The authors declare that they have no known competing financial interests or personal relationships that could have appeared to influence the work reported in this paper.

Acknowledgments

The authors acknowledge the financial support from the National Natural Science Foundation of China (Grant Nos. 11874020 and 12174123).

Appendix A. Supplementary data

Supplementary data to this article can be found online at https://doi.org/10.1016/j.jlumin.2022.118856.

References

[1] Y. Sun, S. Liu, L. Sun, S. Wu, G. Hu, X. Pang, A.T. Smith, C. Hu, S. Zeng, W. Wang, Y. Liu, M. Zheng, Ultralong lifetime and efficient room temperature phosphorescent carbon dots through multi-confinement structure design, Nat. Commun. 11 (2020) 1.
[2] S. Miao, K. Liang, J. Zhu, B. Yang, D. Zhao, B. Kong, Hetero-atom-doped carbon dots: doping strategies, properties and applications, Nano Today 33 (2020) 100879.
[3] Y. Zheng, H. Wei, P. Liang, X. Xu, X. Zhang, H. Li, C. Zhang, C. Hu, X. Zhang, B. Lei, W. Wong, Y. Liu, J. Zhuang, Near-infrared-excited multicolor afterglow in carbon dots-based room-temperature afterglow materials, Angew. Chem. Int. Ed. 133 (2021) 22427–22433.
[4] R. Guo, L. Li, B. Wang, Y. Xiang, G. Zou, Y. Zhu, H. Hou, X. Ji, Functionalized carbon dots for advanced batteries, Energy Storage Mater. 37 (2021) 8.
[5] J. Sun, M. Sadd, P. Edenborg, H. Grönbeck, P.H. Thiesen, Z. Xia, V. Quintano, R. Qiu, A. Matic, V. Palermo, Real-time imaging of Na^+ reversible intercalation in "Janus" graphene stacks for battery applications, Sci. Adv. 7 (2021), eabf0812.
[6] F. Xie, Z. Xu, A.C.S. Jensen, F. Ding, H. Au, J. Feng, H. Luo, M. Qiao, Z. Guo, Y. Lu, A.J. Drew, Y. Hu, M. Titirici, Unveiling the role of hydrothermal carbon dots as anodes in sodium-ion batteries with ultrahigh initial coulombic efficiency, J. Mater. Chem. 7 (2019) 27567.
[7] L. Ye, M. Liao, T. Zhao, H. Sun, Y. Zhao, X. Sun, B. Wang, H. Peng, A sodiophilic interphase-mediated. dendrite-free anode with ultrahigh specific capacity for sodium-metal batteries, Angew. Chem. Int. Ed. 131 (2019) 17210.
[8] Z. Xu, Z. Guo, R. Madhu, F. Xie, R. Chen, J. Wang, M. Tebyetekerwa, Y. Hu, M. Titirici, Homogenous metallic deposition regulated by defect-rich skeletons for sodium metal batteries, Energy Environ. Sci. 14 (2021) 6381.
[9] Z. Liang, X. Fan, W. Zheng, D.J. Singh, Adsorption and formation of small Na clusters on pristine and double-vacancy graphene for anodes of Na-ion batteries, ACS Appl. Mater. Interfaces 9 (2017) 17076.
[10] A.H.F. Niaei, T. Hussain, M. Hankel, D.J. Searles, Hydrogenated defective graphene as an anode material for sodium and calcium ion batteries: a density functional theory study, Carbon 136 (2018) 73–84.
[11] Y. Liu, S. Roy, S. Sarkar, J. Xu, Y. Zhao, J. Zhang, A review of carbon dots and their composite materials for electrochemical energy technologies, Carbon Energy 3 (2021) 795.
[12] Y. Shirasaki, G.J. Supran, M.G. Bawendi, V. Bulović, Emergence of colloidal quantum-dot light-emitting technologies, Nat. Photonics 7 (2013) 13.
[13] H. Shen, W. Cao, N.T. Shewmon, C. Yang, L.S. Li, J. Xue, High-efficiency, low turn-on voltage blue-violet quantum-dot-based light-emitting diodes, Nano Lett. 15 (2015) 1211.
[14] D. Liang, Y. Peng, Y. Fu, M.J. Shearer, J. Zhang, J. Zhai, Y. Zhang, R.J. Hamers, T. L. Andrew, S. Jin, Color-pure violet-light-emitting diodes based on layered lead halide perovskite nanoplates, ACS Nano 10 (2016) 6897.
[15] W. Deng, X. Jin, Y. Lv, X. Zhang, X. Zhang, J. Jie, 2D Ruddlesden–popper perovskite nanoplate based deep-blue light-emitting diodes for light communication, Adv. Funct. Mater. 29 (2019) 1903861.
[16] Y. Jin, Z. Wang, S. Yuan, Q. Wang, C. Qin, K. Wang, C. Dong, M. Li, Y. Liu, L. Liao, Synergistic effect of dual ligands on stable blue quasi-2D perovskite light-emitting diodes, Adv. Funct. Mater. 30 (2020) 1908339.
[17] Z. Ren, L. Li, J. Yu, R. Ma, X. Xiao, R. Chen, K. Wang, X.W. Sun, W. Yin, W.C. H. Choy, Simultaneous low-order phase suppression and defect passivation for efficient and stable blue light-emitting diodes, ACS Energy Lett. 5 (2020) 2569.
[18] Y. Shen, K. Shen, Y. Li, M. Guo, J. Wang, Y. Ye, F. Xie, H. Ren, X. Gao, F. Song, J. Tang, Interfacial potassium-guided grain growth for efficient deep-blue perovskite light-emitting diodes, Adv. Funct. Mater. 31 (2021) 2006736.
[19] S. Yan, W. Tian, H. Chen, K. Tang, T. Lin, G. Zhong, L. Qiu, X. Pan, W. Wang, Deep blue layered lead perovskite light-emitting diode, Adv. Opt. Mater. 9 (2021) 2001709.
[20] H. Jia, Z. Wang, T. Yuan, F. Yuan, X. Li, Y. Li, Z. Tan, L. Fan, S. Yang, Electroluminescent warm white light-emitting diodes based on passivation enabled bright red bandgap emission carbon quantum dots, Adv. Sci. 6 (2019) 1900397.
[21] Q. Wang, Y. Gao, B. Wang, Y. Guo, U. Ahmad, Y. Wang, Y. Wang, H. Li Siyu Lu, G. Zhou, S, N-codoped oil-soluble fluorescent carbon dots for a high color-rendering WLED, J. Mater. Chem. C 8 (2020) 4343.
[22] T. Feng, S. Tao, D. Yue, Q. Zeng, W. Chen, B. Yang, Recent advances in energy conversion applications of carbon dots: from optoelectronic devices to electrocatalysis, Small 16 (2020) 2001295.
[23] S. Zhu, Q. Meng, L. Wang, J. Zhang, Y. Song, H. Jin, K. Zhang, H. Sun, H. Wang, B. Yang, Highly photoluminescent carbon dots for multicolor patterning, sensors, and bioimaging, Angew. Chem. Int. Ed. 125 (2013) 4045.
[24] H. Ding, S. Yu, J. Wei, H. Xiong, Full-color light-emitting carbon dots with a surface-state-controlled luminescence mechanism, ACS Nano 10 (2016) 484.
[25] X. Miao, D. Qu, D. Yang, B. Nie, Y. Zhao, H. Fan, Z. Sun, Synthesis of carbon dots with multiple color emission by controlled graphitization and surface functionalization, Adv. Mater. 30 (2018) 1704740.
[26] H. Yang, Y. Liu, Z. Guo, B. Lei, J. Zhuang, X. Zhang, Z. Liu, C. Hu, Hydrophobic carbon dots with blue dispersed emission and red aggregation-induced emission, Nat. Commun. 10 (2019) 1.
[27] B. Zhao, Z. Wang, Z. Tan, Deep-blue carbon dots offer high colour purity, Nat. Photonics 14 (2020) 130.
[28] F. Yuan, Y. Wang, G. Sharma, Y. Dong, X. Zheng, P. Li, A. Johnston, G. Bappi, J. Z. Fan, H. Kung, B. Chen, M.I. Saidaminov, K. Singh, O. Voznyy, O.M. Bakr, Z. Lu, E.H. Sargent, Bright high-colour-purity deep-blue carbon dot light-emitting diodes via efficient edge amination, Nat. Photonics 14 (2020) 171.
[29] X. Wang, Y. Ma, Q. Wu, Z. Wang, Y. Tao, Y. Zhao, B. Wang, J. Cao, H. Wang, X. Gu, H. Huang, S. Li, X. Wang, F. Hu, M. Shao, L. Liao, T. Sham, Y. Liu, Z. Kang, Ultra-bright and stable pure blue light-emitting diode from O, N co-doped carbon dots, Laser Photon. Rev. 15 (2021) 2000412.
[30] H. Zheng, Q. Wang, Y. Long, H. Zhang, X. Huang, R. Zhu, Enhancing the luminescence of carbon dots with a reduction pathway, Chem. Commun. 47 (2011) 10650.
[31] T.H. Kim, F. Wang, P. McCormick, L. Wang, C. Brown, Q. Li, Salt-embedded carbon nanodots as a UV and thermal stable fluorophore for light-emitting diodes, J. Lumin. 154 (2014) 1.
[32] Q. Xu, Y. Liu, R. Su, L. Cai, B. Li, Y. Zhang, L. Zhang, Y. Wang, Y. Wang, N. Li, X. Gong, Z. Gu, Y. Chen, Y. Tan, C. Dong, T.S. Sreeprasad, Highly fluorescent Zn-doped carbon dots as Fenton reaction-based bio-sensors: an integrative experimental–theoretical consideration, Nanoscale 8 (2016) 17919.
[33] N.U. Ain, M.O. Eriksson, S. Schmidt, M. Asghar, P.C. Lin, P.O. Holtz, M. Syväjärvi, G.R. Yazdi, Tuning the emission energy of chemically doped graphene quantum dots, Nanomaterials 6 (2016) 198.
[34] P. Khare, A. Bhati, S.R. Anand, Gunture, S.K. Sonkar, Brightly fluorescent zinc-doped red-emitting carbon dots for the sunlight-induced photoreduction of Cr (VI) to Cr (III), ACS Omega 3 (2018) 5187.
[35] Q. Xu, R. Su, Y. Chen, S.T. Sreenivasan, N. Li, X. Zheng, J. Zhu, H. Pan, W. Li, C. Xu, Z. Xia, L. Dai, Metal charge transfer doped carbon dots with reversibly switchable, ultra-high quantum yield photoluminescence, ACS Appl. Nano Mater. 1 (2018) 1886.
[36] P. Zhu, Z. Cheng, L. Du, Q. Chen, K. Tan, Synthesis of the Cu-doped dual-emission fluorescent carbon dots and its analytical application, Langmuir 34 (2018) 9982.

[37] W. Zhang, Y. Ni, X. Xu, W. Lu, P. Ren, P. Yan, C.K. Siu, S. Ruana, S.F. Yu, Realization of multiphoton lasing from carbon nanodot microcavities, Nanoscale 9 (2017) 5963.
[38] K. Jiang, S. Hu, Y. Wang, Z. Li, H. Lin, Photo-stimulated polychromatic room temperature phosphorescence of carbon dots, Small 16 (2020) 2001909.
[39] S. Fujisawa, Y. Okita, H. Fukuzumi, T. Saito, A. Isogai, Preparation and characterization of TEMPO-oxidized cellulose nanofibril films with free carboxyl groups, Carbohydr. Polym. 84 (2011) 579.
[40] X. Chen, W. Wu, W. Zhang, Z. Wang, Z. Fu, L. Zhou, Z. Yi, G. Li, L. Zeng, Blue and green double band luminescent carbon quantum dots: synthesis, origin of photoluminescence, and application in white light-emitting devices, Appl. Phys. Lett. 118 (2021) 153102.
[41] Z.L. Wu, M.X. Gao, T.T. Wang, X.Y. Wan, L.L. Zheng, C.Z. Huang, A general quantitative pH sensor developed with dicyandiamide N-doped high quantum yield graphene quantum dots, Nanoscale 6 (2014) 3868.
[42] Y. Wang, Y. Zhang, M. Jia, H. Meng, H. Li, Y. Guan, L. Feng, Functionalization of carbonaceous nanodots from MnII-coordinating functional knots, Chem. Eur J. 21 (2015) 14843.
[43] P. Yu, X. Wen, Y.R. Toh, J. Tang, Temperature-dependent fluorescence in carbon dots, J. Phys. Chem. C 116 (2012) 25552.
[44] Y. Zhang, Y. Hu, J. Lin, Y. Fan, Y. Li, Y. Lv, X. Liu, Excitation wavelength independence: toward low-threshold amplified spontaneous emission from carbon nanodots, ACS Appl. Mater. Interfaces 8 (2016) 25454.
[45] W.F. Zhang, L.B. Tang, S.F. Yu, S. Pi Lau, Observation of white-light amplified spontaneous emission from carbon nanodots under laser excitation, Opt. Mater. Express 2 (2012) 490.
[46] Z. Lin, H. Li, R. Huang, Y. Zhang, J. Song, H. Li, Y. Guo, C. Song, J. Robertson, Defect emission and optical gain in SiCxOy: H films, ACS Appl. Mater. Interfaces 9 (2017) 22725.